JACS
JOURNAL OF THE AMERICAN CHEMICAL SOCIETY

Subscriber access provided by BIU Pharmacie | Faculté de Pharmacie, Université Paris V

Article

Thermally Activated Delayed Fluorescent Donor–Acceptor–Donor–Acceptor #-Conjugated Macrocycle for Organic Light-Emitting Diodes

Saika Izumi, Heather F. Higginbotham, Aleksandra Nyga, Patrycja Stachelek, Norimitsu Tohnai, Piotr de Silva, Przemyslaw Data, Youhei Takeda, and Satoshi Minakata

J. Am. Chem. Soc., **Just Accepted Manuscript** • Publication Date (Web): 02 Jan 2020

Downloaded from pubs.acs.org on January 2, 2020

Just Accepted

"Just Accepted" manuscripts have been peer-reviewed and accepted for publication. They are posted online prior to technical editing, formatting for publication and author proofing. The American Chemical Society provides "Just Accepted" as a service to the research community to expedite the dissemination of scientific material as soon as possible after acceptance. "Just Accepted" manuscripts appear in full in PDF format accompanied by an HTML abstract. "Just Accepted" manuscripts have been fully peer reviewed, but should not be considered the official version of record. They are citable by the Digital Object Identifier (DOI®). "Just Accepted" is an optional service offered to authors. Therefore, the "Just Accepted" Web site may not include all articles that will be published in the journal. After a manuscript is technically edited and formatted, it will be removed from the "Just Accepted" Web site and published as an ASAP article. Note that technical editing may introduce minor changes to the manuscript text and/or graphics which could affect content, and all legal disclaimers and ethical guidelines that apply to the journal pertain. ACS cannot be held responsible for errors or consequences arising from the use of information contained in these "Just Accepted" manuscripts.

is published by the American Chemical Society. 1155 Sixteenth Street N.W., Washington, DC 20036

Published by American Chemical Society. Copyright © American Chemical Society. However, no copyright claim is made to original U.S. Government works, or works produced by employees of any Commonwealth realm Crown government in the course of their duties.

Thermally Activated Delayed Fluorescent Donor–Acceptor–Donor–Acceptor π-Conjugated Macrocycle for Organic Light-Emitting Diodes

Saika Izumi,[†] Heather F. Higginbotham,[‡] Aleksandra Nyga,[‖] Patrycja Stachelek,[§] Norimitsu Tohnai,[#] Piotr de Silva,[⊥] Przemyslaw Data,*[,§,‖,▽] Youhei Takeda,*[,†] and Satoshi Minakata*[,†]

[†] Department of Applied Chemistry, Graduate School of Engineering, Osaka University, Yamadaoka 2-1, Suita, Osaka 565-0871, Japan

[‡] School of Chemistry, Monash University, Clayton Victoria 3800, Australia

[‖] Faculty of Chemistry, Silesian University of Technology, M. Strzody 9, 44-100 Gliwice, Poland

[§] Durham University, Physics Department, South Road, Durham DH1 3LE, United Kingdom

[#] Department of Material and Life Science, Graduate School of Engineering, Osaka University, Yamadaoka 2-1, Suita, Osaka 565-0871, Japan

[⊥] Department of Energy Conversion and Storage, Technical University of Denmark, Anker Engelunds Vej 301, 2800 Kongens Lyngby, Denmark

[▽] Center of Polymer and Carbon Materials, Polish Academy of Sciences, M. Curie-Sklodowskiej 34, 41-819 Zabrze, Poland

ABSTRACT: A new class of thermally activated delayed fluorescent donor–acceptor–donor–acceptor (D–A–D–A) π-conjugated macrocycle comprised of two U-shaped electron-acceptors (dibenzo[*a,j*]phenazine) and two electron-donors (*N,N'*-diphenyl-*p*-phenyelendiamine) has been rationally designed and successfully synthesized. The macrocyclic compound displayed polymorphs-dependent conformations and emission properties. Comparative studies on physicochemical properties of the macrocycle with a linear surrogate has revealed significant effects of the structural cyclization of D–A-repeating structure, including more efficient thermally activated delayed fluorescence (TADF). Furthermore, an organic light-emitting diode (OLED) device fabricated with the macrocycle compound as the emitter has achieved a high external quantum efficiency (EQE) up to 11.6%, far exceeding the theoretical maximum (5%) of conventional fluorescent emitters and that with linear analog (6.9%).

INTRODUCTION

Organic π-conjugated oligomers and polymers play crucial roles in materials science, finding a number of applications such as chemical sensors,[1] bio-imaging,[2] organic field-effect transistors (OFETs),[3] organic photovoltaics (OPVs),[4] and organic light-emitting diodes (OLEDs).[5] Their photophysical and redox properties are finely tunable through exquisite modifications of structure, electronic bias, and conjugation length of π-conjugated systems, in accordance with the intended function. The topological aspect also significantly matters in their functions. Organic π-conjugated macrocycles, which are regarded as terminal-less counterparts of linear π-conjugated oligomers and polymers, have emerged as unique organic functional materials.[6,7] They can display not only unique photophysical and redox properties but also highly-ordered 2D- and 3D-aligned molecular assemblies otherwise difficult to achieve with linear π-conjugate systems, arising from their specific structural motifs such as bent, curved, and/or twisted π-systems as well as well-defined cavities.[6] To date, a great number of structurally well-defined π-conjugated macrocycles, particularly, hydrocarbon-based π-conjugated macrocycles assembled from (hetero)arylenes, ethynylenes, and vinylenes, have been developed, and their optoelectronic properties have been intensively studied in the context of partial motifs of carbon materials.[7]

In sharp contrast, π-conjugated macrocycles comprised of π-electronic donors (D) and acceptors (A) (i.e., D–A-embedded π-conjugated macrocycles) have been less developed, and therefore their optoelectronic properties have been less investigated,[8] although the incorporation of D and A moieties in π-conjugated main frameworks is a powerful strategy for tuning photophysical and redox properties of linear π-conjugated oligomers and polymers in material science. In 2012, Jäkle developed ambipolar B–π–N macrocycles, uncovering unique Lewis-base-responsive photoluminescent behavior.[9] In 2015, Jasti[10a] and Itami[10b] independently developed an electron-deficient arene-incorporated cycloparaphenylenes (CPPs), which are featured with the narrower HOMO/LUMO band gaps than those with the same ring-size all-carbon CPPs. The Nuckolls group has intensively developed D–A-repeating carbon nanohoops comprised of multiple D–A units (D = bithiophene derivatives; A = perylene diimides).[11] Notably, the validity of the D–A-repeating π-conjugated macrocycles as functional materials has been demonstrated by applying the macrocycles to OFETs,[11e] a bulk heterojunction OPVs,[11b] and organic capsule transistors for sensing chemicals.[11d] Therefore, the development of novel D–A π-conjugated macrocycles and the exploration of their potency as optoelectronic materials would offer significant opportunities for tailoring optoelectronic properties by fluctuating three-dimensional shapes (e.g., bent, curved, and twisted confor-

mations) and by utilizing exterior/interior π-π interactions and/or host-guest interactions otherwise difficult to realize with flat and fully-π-conjugated systems. However, it should be stated that the synthesis of new π-conjugated macrocycles still remains a challenge in itself, mainly due to limited synthetic strategies and building blocks suitable for π-conjugated macrocycles. The rational design of D–A π-conjugated macrocycles that simultaneously satisfy requirements for desired functions and synthetic feasibility is to be devised.

Thermally activated delay fluorescence (TADF) is a unique photophysical phenomena and promising for enhancing external quantum efficiency (EQE) of organic light-emitting diodes (OLEDs), because TADF-active organic emitters can theoretically harvest 100% excitons generated in the emitting layer by electrical excitation and convert into light through efficient reverse intersystem crossing (rISC).[12] The key issues in designing efficient TADF emitters include how to accelerate spin-forbidden and endothermic rISC process ($T_1 \rightarrow S_1$). D–A π-conjugated systems with a large D–A dihedral angle and with a vibrational motion can provide a solution, minimizing singlet-triplet energy gap (ΔE_{ST}) to lower activation energy for rISC and mixing excited CT and LE states to allow spin-flip electronic transitions.[12c] Therefore, a myriad of TADF organic materials have been developed based on linear or branched D–A scaffolds.[12] In sharp contrast, macrocyclic TADF materials have been rarely explored.[13–15] In 2009, Adachi realized the first TADF-OLEDs using Sn^{4+}-porphyrin complexes as the emitter, which also represents the first example of macrocyclic organic TADF material.[13] However, the emitters contain environmentally unbenign metal ion, and the TADF emission is very faint. In 2014, Kanbara revealed the delayed fluorescence behavior of azacalix[*n*](2,6)pyridines (*n* = 3, 4), which represents the first example of D–A-repeating organic TADF macrocycles.[14] Yet, the rather large ΔE_{ST} (calc.) values (>600 meV) of the azacalixpyridines suggested that a harsh thermal reverse internal conversion (RIC) from T_1 to T_n is required for rISC process. More recently, the Su and Huang developed a pure organic deep-blue TADF emitting compound comprising triarylamines bridged with electron-withdrawing SO_2 group.[15] In addition to the scarcity of macrocyclic TADF-active compounds, to the best of our knowledge, the EQEs of OLEDs fabricated with any macrocyclic TADF emitters have never been clarified. Furthermore, the influence of the macrocyclization of linear D–A-repeating π-conjugated systems on their physicochemical properties, especially TADF behavior, has remained an open question.

Herein we disclose the development of a purely organic macrocyclic D–A–D–A π-conjugated macrocycle **1** (Figure 1a), which displays efficient TADF emissions. From the comparison of its physicochemical properties with those of linear analog **2** (Figure 1b), the macrocyclization effect on its physicochemical properties was revealed. Most importantly, the OLEDs fabricated with the developed macrocyclic compound **1** as a TADF emitter achieved as high EQE as 11.6%, exceeding the theoretical maximum (5%)[16] of that utilizing conventional fluorescent emitters and that with linear material **2** (6.8%).

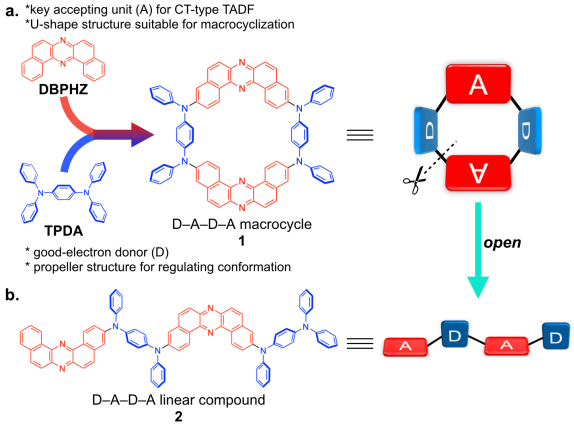

Figure 1. Designed (a) macrocycle **1** and (b) linear analog **2**.

RESULTS and DISCUSSION

Design and Synthesis. We designed D–A–D–A macrocycle **1**, comprising two *p*-phenylenediamine derivative as the donors and two dibenzo[*a,j*]phenazine (DBPHZ)[17] as the acceptors, as TADF π-conjugated macrocyclic compound (Figure 1a). As our research program of developing multi-photofunctional organic materials, we have demonstrated that DBPHZ-cored twisted donor–acceptor–donor (D–A–D) scaffold holds great promise for realizing efficient thermally activated delayed fluorescence (TADF),[18] multi-color-changing mechanochromic luminescence (MCL),[18b,d] and room temperature phosphorescence (RTP).[18c,d] In particular, it is noted that the DBPHZ core (Figure 1a) plays an important role in TADF and RTP functions: the lowest triplet excited state (T_1) of the D–A–D family is exclusively localized on the DBPHZ acceptor unit (^3LE_A), which allows narrowing the ΔE_{ST} of the molecules by adjusting the ^{1}CT energy levels though fluctuation of electronic bias and D–A dihedral angles. On one hand, the U-shaped structure of DBPHZ can be suitable for the formation of macrocyclic structure. Therefore, we envisaged that a twisted D–A–D–A macrocycle composed of two DBPHZs (A) and two bridging electron donors (D) should serve as an efficient TADF π-conjugated macrocyclic material (Figure 1a). From the viewpoint of synthetic feasibility, appropriate selection of bridging donors would be highly important. The structural pre-organization required for macrocyclization is highly dependent on the conformation and configuration of the precursor/intermediate. Otherwise, undesired intermolecular oligomerization/polymerization over desired intramolecular cyclization can occur.[19] Since triarylamines take propeller-like geometries,[20] we envisioned that the incorporation of *N,N,N',N'*-tetraphenylene-1,4-diamine (TPDA, Figure 1a) motif into macrocyclic structure would allow for regulating conformational flexibility of a precursor for macrocyclization (corresponding to **6** in Scheme 1) and facilitating the cyclization process. Also, the bridging with a heteroatom (N) would allow for twisting of π-conjugated panels and alleviating ring strain in forming macrocycle **1**. To investigate the effect of macrocyclization of a D–A–D–A scaffold on is physicochemical properties, a linear analog **2** (i.e., the open form of **1**) was also designed (Figure 1b).

Scheme 1. Divergent synthetic routes to **1** and **2**.

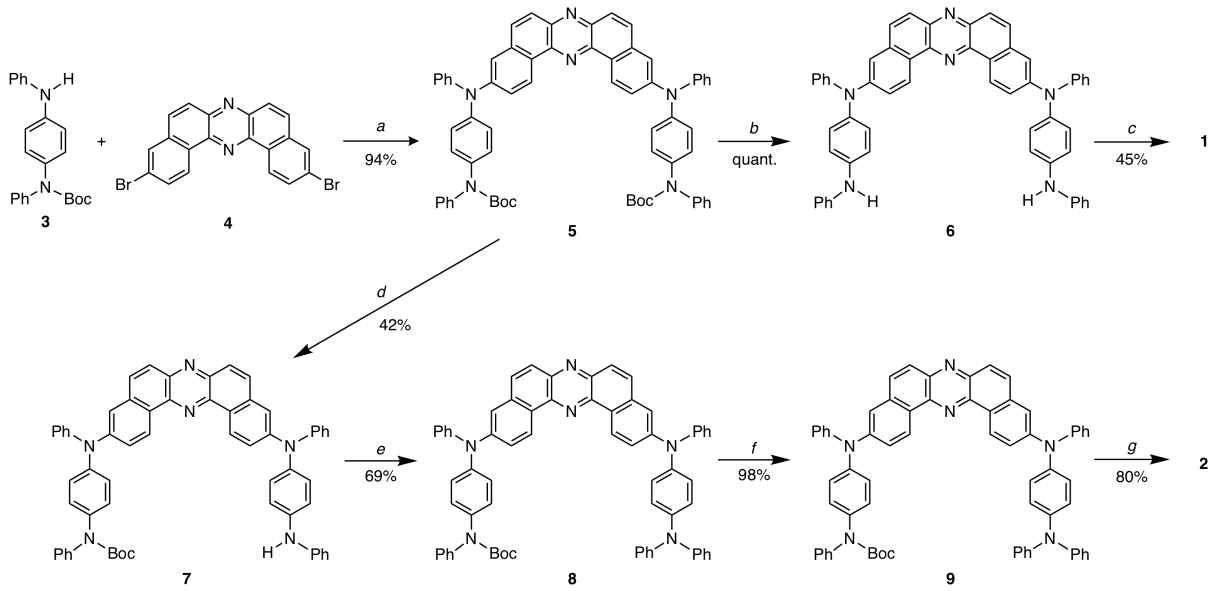

Reagents and conditions: (a) $Pd_2(dba)_3$ (1 mol%), QPhos (4 mol%), NaO*t*-Bu (2.2 equiv), toluene, 60 °C, 12 h. (b) TFA (excess), CH_2Cl_2, r.t., 40 min. (c) **4** (1.0 equiv), $Pd_2(dba)_3$ (5 mol%), QPhos (20 mol%), K_2CO_3 (2.2 equiv), 1,4-dioxane, 100 °C, 24 h. (d) TFA (8.0 equiv), CH_2Cl_2, r.t., 30 min. (e) PhBr (1.0 equiv), $Pd[P(t\text{-}Bu)_3]_2$ (10 mol%), K_2CO_3 (3.0 equiv), 1,4-dioxane, 100 °C, 24 h. (f) TFA (excess), CH_2Cl_2, r.t., 30 min. (g) dibenzo[*a,j*]phenazin-3-yl trifluoromethanesulfonate (1.5 equiv), $Pd_2(dba)_3$ (5 mol%), SPhos (15 mol%), K_2CO_3 (1.5 equiv), 1,4-dioxane, 100 °C, 24 h.

Macrocycle **1** and its linear analog **2** were successfully synthesized in a divergent fashion by applying common intermediate **5** (Scheme 1, for the detailed synthetic conditions and procedures, see the Supporting Information). Starting from a commercially available *N*-phenyl-*p*-phenylenediamine, donor **3** was prepared in 65% yield (in 4 steps), by modifying synthetic methods for oligo(*p*-aniline) compounds (for the details, see the SI).[21] The donor **3** was attached to the DBPHZ acceptor through a double Pd-catalyzed Buchwald-Hartwig amination with 3,11-dibromodibenzophenazine **4** using a bulky phosphine ligand (Qphos)[22] to give the common intermediate **5** in a high yield. The deprotection of the N-Boc groups of **5** with an excess amount of trifluoroacetic acid (TFA) quantitatively afforded macrocycle precursor **6**. Notably, macrocyclization was successfully achieved through a Pd-catalyzed Buchwald-Hartwig double amination of **4** with the D–A–D precursor **6** in 45%, which represents a relatively high yield in cyclization of aromatic components. On one hand, mono-deprotection of the N-Boc groups of **5** with 8 equivalents of TFA gave intermediate **7**, which was then N-phenylated with bromobenzene to provide **8** in a good yield. The deprotection of the remaining N-Boc group of **8** followed by the Buchwald-Hartwig amination with a DBPHZ having an OTf group at the 3-position successfully completed the synthesis of linear analog **2**. All the newly synthesized compounds were fully characterized by spectroscopic data (e.g., ^1H & ^{13}C NMR, IR, MS, and HRMS; for the details, see the SI).

Polymorphism and Single Crystal X-ray Crystallographic Analyses. The macrocycle **1** formed two polymorphs depending on recrystallization conditions: Orange prism crystals (denoted as "polymorph **1**-O") were grown from a *n*-hexane/$CHCl_3$ biphasic solution through a liquid-liquid diffusion technique, while deep-red prism crystals (denoted as "polymorph **1**-R") formed through slow evaporation of a $CHCl_3$ solution of **1** over 2 weeks. Importantly, the X-ray crystallographic analyses of the single crystals revealed the differences in molecular geometries and packing structures (Figure 2), which would give significant influences on photophysical properties.[23] The polymorph **1**-O crystallized in the triclinic space group *P*1 and exhibited weak orange emission (λ_{max} = 594 nm, Φ_{PL} = 0.01, for the PL spectra, see the Figure S7a). In the crystal, the macrocycle takes a highly symmetric structure with the symmetric center (*i*) (Figure 2a). As designed, the donor units take propeller-structure, with the twisting angles between the phenylene and external N-phenyl planes being 85.6° and 88.9° (Figure 2b). Also, the phenylene planes of the donors are twisted against the DBPHZ acceptor unit, with the dihedral angle between the phenylene plane and the terminal benzene unit of the DBPHZ being 56.9° and 62.8°. More interestingly, both DBPHZ units take helically twisted structure, with the dihedral angle between the terminal fused benzene rings being 17.4° (Figure 2b), where the central phenazine unit is nearly flat (deviation angle: 5.9°). The twisting of the DBPHZ would indicate a large strain accommodated into the molecule by the macrocyclization. In the crystal polymorph **1**-O, the macrocycle molecules align along the *c* axis, and the highly organized assemblies form porous columns with the cavity diameter of 6.58 Å, where chloroform molecules are trapped within the cavity (Figure 2c). On close inspection of the columns, the benzo[*f*]quinoxaline moieties of the DBPHZ unit are contiguously stacked in a face-to-face manner with a very close interplane distance (3.39 Å), indicating the operation of a strong electronic interaction between the molecules through π-orbitals.

The polymorph **1**-R formed a monoclinic system with the space group $P2_1/m$ and exhibited red emission (λ_{max} = 654 nm, Φ_{PL} = 0.01, for the PL spectra, see the Figure S7a). Most importantly, the macrocycle takes a saddle-shaped conformation (Figure 2d and e). The phenylene donor units once again take propeller shape (the twisting angles between the phenylene and external N-phenyl planes range from 72.8° to 82.3°), and the phenylene unit is more twisted against the acceptor than polymorph **1**-O (the dihedral angle between the phenylene plane and

the terminal benzene unit of the DBPHZ: 66.6°). In sharp contrast to polymorph **1**-O, the DBPHZ units of the macrocycle in polymorph **1**-R is planar (Figure 2e). The less distortion of the DBPHZ units indicated that the conformation in polymorph **1**-R is thermodynamically more stable than that in polymorph **1**-O, which was indeed supported by theoretical calculation by the DFT method (see the following section and the SI). Each porous column aligned along the *a* axis in polymorph **1**-R are independent from each other, with voids between each column being filled with chloroform molecules (Figure 2f). Interestingly, each column is formed by the assembly of dimeric pairs of the macrocycle, where four D•••A pairs are stacked with a very close distance (the interplane distances between the phenylene and the DBPHZ plane: 2.98–3.18 Å, Figure 2f), suggesting strong intermolecular charge-transfer interactions between the two molecules. This would be in consistent with a drastic change in crystal color and emission wavelength from polymorph **1**-O. Single crystals of linear compound **2** suitable for the X-ray single-crystal analysis were not obtained regardless of a number of attempts, implying more flexibility of the conformations than cyclic compound **1**. The solids of linear compound **2** displayed an orange PL (λ_{max} = 605 nm, Φ_{PL} = 0.08, for the PL spectra, see the Figure S7b in the SI) with a slightly higher PLQY than those of polymorphs **1**-R and **1**-O. This would indicate that the strong electronic interactions of macrocycle quench PL in the crystals.

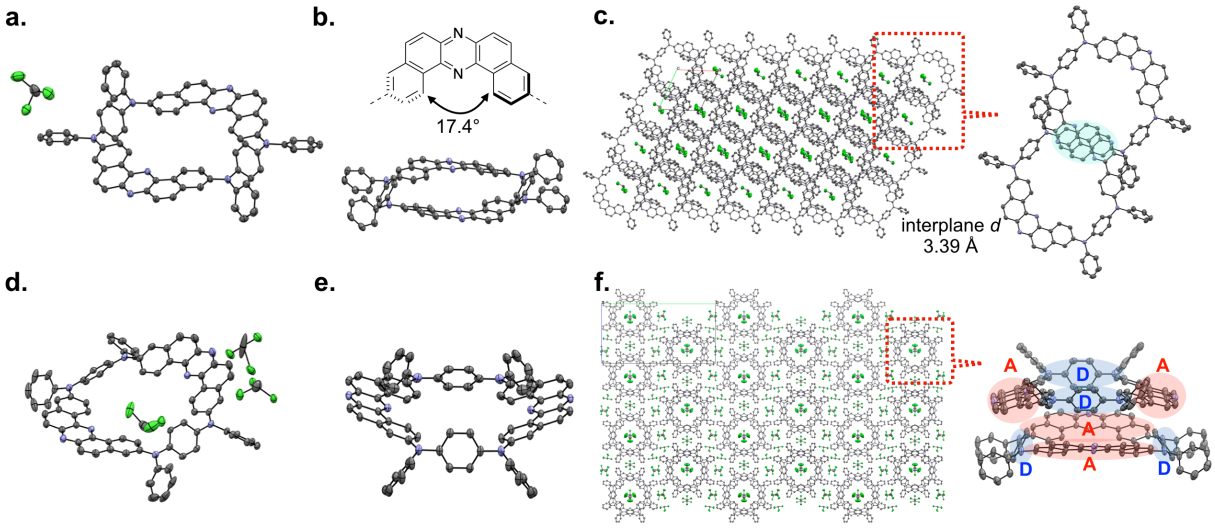

Figure 2. ORTEP drawings of **1** in (a)–(c) polymorph **1**-O and (d)–(f) polymorph **1**-R: (a), (d) molecular structures; (b), (e) side views; (c), (f) packing structures (thermal ellipsoids are set at the 50% probability level). The hydrogen atom and partial crystal solvent $CHCl_3$ were omitted for clarity.

Steady-State Absorption and Photoluminescence Properties in Solutions. To reveal the photophysical properties of **1** and **2** in solution, steady-state UV-vis absorption and photoluminescence spectra of their diluted solutions (cyclohexane, toluene, THF, CH_2Cl_2 and $CHCl_3$) were investigated (Figure 3, for the summarized data, see the Table 1). As a whole, the line shapes, the maximum absorption wavelengths (λ_{abs}), and molar absorption coefficients (ε) of the UV-vis absorption spectra of diluted solutions of **1** were not significantly affected by the difference in polarity of solvents used (Figure 3a). However, on close inspection of the absorption onsets of solutions of **1**, a slight red-shift as a function of solvent polarity was observed (Figure 3a). In conjunction with a relatively large ε value (*ca.* 50,000 $M^{-1}cm^{-1}$) of the absorption peaked at around 470 nm and the absence of the corresponding peak in the absorption spectra of DBPHZ[17] and TPDA[24] in the region (400–550 nm), the electronic transition observed at around 470 nm has the mixed character of intramolecular charge-transfer (ICT) and π-π* transition, or hybrid CT (Figure 3). This was also supported by the TD-DFT calculations (*vide infra*). The diluted solutions of linear compound **2** also displayed similar absorption spectra with an ICT peak (λ_{abs} 477–485 nm) and the π-π* transition (λ_{abs} 332–337 nm) ascribed to the TPDA unit with a slightly smaller ε with a broader band than that of **1** (Figure 3b), which could indicate the fluctuation of the conformers.

Upon the irradiation of UV light, the cyclohexane solution of **1** displayed bright green emission from the singlet charge-transfer excited state (^{1}CT) state (λ_{em} 540 nm) with a moderate photoluminescence quantum yield (Φ_{PL} 0.31) (Figure 3a). In a slightly polar solvent (toluene), the macrocycle exhibited orange emission (λ_{em} 595 nm, Φ_{PL} 0.28) from the more stabilized ^{1}CT state. In the case of more polar solvents (e.g. THF, CH_2Cl_2, and $CHCl_3$), no emission was observed, indicating strong ICT nature in the excited states of the macrocycle.[18] The cyclohexane solution of **2** displayed a very similar green emission (λ_{em} 534 nm) with that of **1**, but with a higher Φ_{PL} (0.53) (Figure 3b and Table 1). Notably, the emission in toluene showed a red emission (λ_{em} 615 nm) with a lower Φ_{PL} (0.20) (Figure 3b and Table 1). It should be noted that the larger red-shift in emission (λ_{em} 2466 cm^{-1} for **2** *vs* 1712 cm^{-1} for **1**) would indicate much more flexibility of conformation of **2** in the excited states, probably due to free D–A rotation that should lead to the dissipation of the excited energies through thermal processes.[25]

Since TADF is irradiated by way of the excited triplet states, the intensity of the TADF is very sensitive toward the presence of oxygen gas (O_2), which can efficiently quench the excited triplet states through non-irradiative pathways. To investigate how much TADF contributes to the PL of **1** and **2** in solution, the steady-state PL spectra of toluene solutions of **1** and **2** were measured in the presence and absence of O_2 (Figure 3c and

d). Upon degassing, a significant increase (66%) in emission intensity was observed for macrocycle **1**, when compared to an aerated condition (Figure 3c). In contrast, linear analog **2** showed only a 24% increase in emission intensity (Figure 3d). Assuming that the outputs observed under aerated and degassed conditions can be related to the prompt fluorescence (PF) and the sum of the PF and the delayed fluorescence (DF) after an excursion to the triplet state, respectively, the number expressed by the following equation {(DF/PF)–1}×100 (%) would indicate the % of the harvested triplet in a form of DF. Given the DF/PF ratio of **1** and **2**, macrocyclic compound **1** is much more promising TADF material than **2**, which was supported by the time-resolved spectroscopic analyses and OLED performances (*vide infra*).

Table 1. Steady-state photophysical data of diluted solutions of **1** and **2**.

compound	solvent[a]	λ_{abs} (nm)	λ_{em} (nm)	Φ_{PL}[b]
1	cyclohexane[c]	268, 338, 370, 476	540	0.31
	toluene	283, 336, 367, 473	595	0.28
	THF	280, 335, 366, 474	ND	<0.01
	CH_2Cl_2	281, 335, 368, 476	ND	<0.01
	$CHCl_3$	281, 339, 369, 478	ND	<0.01
2	cyclohexane[c]	286, 334, 475	534	0.53
	toluene	289, 336, 479	615	0.20
	THF	286, 332, 477	ND	<0.01
	CH_2Cl_2	288, 334, 479	ND	<0.01
	$CHCl_3$	288, 337, 485	ND	<0.01

[a]Concentration: 10^{-5} M. [b]Determined with an integrated sphere. [c]Saturated solution was used, due to the low solubility in cyclohexane (concentration < 10^{-6} M).

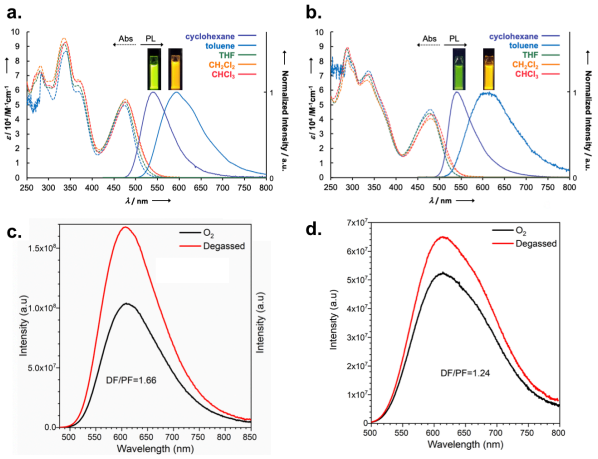

Figure 3. Steady-state UV-vis absorption (Abs) and photoluminescence (PL) spectra of dilute solutions (purple: cyclohexane; sky blue: toluene; green: THF; orange: CH_2Cl_2; red: $CHCl_3$) of (a) macrocycle **1** and (b) linear analog **2** (λ_{ex} = 340 nm, concentrations: 10^{-6}–10^{-5} M). Absorption spectra of cyclohexane solutions of **1** and **2** are not shown, due to the uncertainty of the exact concentration. PL spectra of the toluene solutions (5 μM) of (c) **1** and (d) **2** with aerated (black lines) and degassed (red lines) (λ_{ex} = 470 nm).

Electrochemical Properties. The electrochemical properties of macrocycle **1** and linear analog **2** were investigated with cyclic voltammetry (CV) (Figure 4). Both compounds exhibited a reversible one-step reduction ($^{red}E_{1/2}$ = –1.88 V for **1**; –1.89 V for **2** *vs* Fc/Fc^+) and a two-step oxidation process ($^{ox1}E_{1/2}$ = +0.27 V for **1**; +0.22 V for **2** *vs* Fc/Fc+, $^{ox2}E_{1/2}$ = +0.69 V for **1**; +0.63 V for **2** *vs* Fc/Fc^+) (Figure 4), indicating their high electrochemical stabilities suitable for carrier injection/transportation as optoelectronic materials. The ionization potential (IP)/electron affinity (EA) of **1** and **2** determined by the CV experiment are 5.37 eV/3.22 eV and 5.32 eV/3.21 eV, respectively. The $^{red}E_{1/2}$ potentials (*vs* Fc/Fc^+) of **1** and **2** are very close to that of DBPHZ (–1.88 V),[17] while the $^{ox1}E_{1/2}$ of **1** and **2** are slightly negatively shifted against that of TPDA (+0.18 V).[26] This negative shift of $^{ox1}E_{1/2}$ would be rationalized by the existence of electron-withdrawing aryl moieties (DBPHZ) on the donor units.[27] Therefore, these data would suggest the localization of the HOMO and LUMO orbitals of both compounds on the donors and acceptors, respectively, which is in good agreement of the theoretical calculation (Figure 5, *vide infra*).

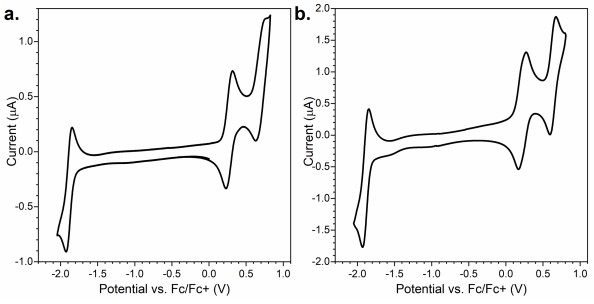

Figure 4. Cyclic voltammograms of (a) macrocycle **1** (5×10^{-4} M) and (b) linear compound **2** (1×10^{-3} M) in CH_2Cl_2 containing 0.1 M Bu_4NBF_4. Electrodes: working (Pt), counter (Pt wire), reference (Ag/AgCl). Scan rate: 50 mV s^{-1}.

Theoretical Calculation. To obtain insights into the conformations and electronic structure of the macrocycle and linear analog, theoretical calculations using the DFT method were performed (Figure 5; for the details, see the SI). The structural optimization of macrocycle **1** was conducted with the geometries obtained from the X-ray crystallographic analyses (for the details, see the SI). The comparison of the energies of helical-type conformer (denoted as "**helical**") related to that found in the polymorph **1**-O (Figure 2a–c) and saddle-type conformer (denoted as "**saddle**") related to that found in the polymorph **1**-R (Figure 2d–f), revealed that there is a large energy difference between these conformers (**helical** has approximately 5 kcal/mol higher energy than **saddle**. For detailed values, see Table S3 in the SI). This suggests that the >99% of the macrocycle **1** takes the saddle-like conformation as the single molecule. This thermodynamic preference of the **saddle** conformer would rationally explain the experimental observation that polymorph **1**-O (**helical** conformer) was obtained under kinetic crystallization conditions, while polymorph **1**-R (**saddle** conformer) was formed under thermodynamic conditions, although packing effect cannot be totally excluded. For both conformers of the macrocycle, the HOMO and HOMO–1 orbitals are delocalized over the entire ring, whereas the LUMO and LUMO+1 orbitals are mostly on the acceptors (Figure 5a). The localization of unoccupied frontier orbitals is more pronounced for the **saddle** conformer. For the linear analogue **2**, the conformational search found that the most stable conformer takes a twisted geometry (Figure 5b). The occupied frontier orbitals are rather delocalized; however, most of the amplitude is clearly localized on the donor. The unoccupied frontier orbitals are mostly localized on the acceptor units, similar as for the macrocycles.

The excited state calculations with time-dependent DFT (TD-DFT) indicated that the lowest singlet excited state for both conformers of **1** is dominated by the HOMO→LUMO transition but is symmetrically-forbidden (red arrows in Figure 5a). The second and third electronic transitions are allowed and dominated by HOMO→LUMO+1 (green arrows) and HOMO–1→LUMO (blue arrows) transitions, respectively (Figure 5a). The comparison of the calculated and experimental UV-vis spectra (Figure S8 in the SI) for both conformers of **1** in toluene indicates that the saddle-type conformer is dominant in diluted solutions. This is supported by the closer match of the lowest absorption peak as well as the fact that only the calculated spectrum for the **saddle** shows a double peak in the 300-400 nm range (Figure S8b). The comparison of the spectra is also consistent with the thermodynamic stability of both conformers. The TD-DFT calculation for the energetically-lowest conformer of **2** suggested that the absorption peak at around 480 nm is composed of three nearly-lying excitations which are dominated by the HOMO–1→LUMO, HOMO→LUMO+1, and HOMO–1→LUMO+1 transitions, respectively. The calculated spectrum also matches the experimental spectrum rather well (Figure S9 in the SI). In particular, the predicted absorption peak is at 485 nm which is very close to the experimental one at 479 nm. Considering that the experimental lowest-lying absorption peaks of **1** and **2** are very close to each other, the fact that the calculated peaks of **saddle** and the conformer of **2** differ noticeably can be attributed to the importance of vibronic effects. Indeed, the symmetry-forbidden transition to S1 in **saddle** is at 476 nm, almost on top of the experimental peak. Therefore, mixing of electronic states due to vibrations would make the transition to S1 allowed akin to the transitions in the linear analogue. This would lead to the red shift of the calculated band and increase of its intensity, thereby improving the agreement with the experiment. An analogous mixing of states to make forbidden transitions allowed has been recently proposed in the four-state model of TADF to explain the possibility of simultaneous efficient rISC and fluorescence in donor-acceptor TADF emitters.[28] The ΔE_{ST} values calculated using the optimized ground state structures for **helical** and **saddle** conformers (Table S4 and S5 in the SI) were found to be 0.55 eV and 0.50 eV, respectively. These values are relatively large when compared to the experimental gaps obtained with time-resolved emission spectroscopy (*vide infra*), which suggests that the excited state relaxation plays an important role in the emission process.

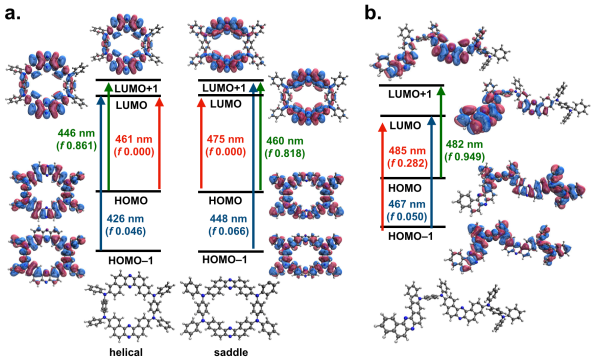

Figure 5. An illustrative summary of the theoretical calculations for (a) helical and saddle-shaped conformers of **1** and (b) **2** at the ω*PBE/cc-pVDZ level. The first 3 vertical electronic transitions are shown in red, green, and blue arrows.

Time-Resolved Spectroscopic Analysis in Host Matrices. To investigate the TADF properties of compounds **1** and **2**, time-resolved luminescence spectroscopic analyses of both compounds in a non-polar Zeonex® and 4,4'-bis(carbazole-9-yl)biphenyl (CBP) host matrices were performed (Figure 6 and 7). In both host matrices, both compounds displayed emissions in two distinct time regions (Figure 7). The first component, decaying with a lifetime in the nanosecond time regime in all the materials, is attributed to prompt fluorescence (PF) from the singlet excited state (S_1), due to the independent emission profiles on temperatures (Figure 6 and 7). In both cases (**1** and **2**), the spectra at the time delay (TD) of 15 ns in both Zeonex® and CBP showed single Gaussian-type spectra ascribed to charge transfer (^{1}CT) emission that decays over longer times (black lines, Figure 6). At a longer delay time in the micro- and millisecond time regions, delayed emissions were observed (Figure 7). Depending on the experimental temperature, both the singlet state delayed emission and triplet state emission were observed on similar millisecond timescales. Therefore, emission from each state is most easily elucidated upon spectral inspection at different temperatures. At room temperature, the delayed emission was observed with the same spectral shape and onset energy as the prompt ^{1}CT spectra (red lines, Figure 6), which was identified as TADF. This assignment as TADF was also confirmed with the linear power dependence of the integrated emission intensity in the millisecond region of **1** and **2** on laser pulse fluence (Figure S10 and S11 in the SI).

On one hand, the emissions from the triplet state was observed at low temperatures (blue lines, Figure 6), with the triplet energy (E_{T1}) for **1** being 2.19 eV in both Zeonex® and CBP hosts (Figure 6a and c). Due to the polarity of CBP host, the ^{1}CT energy of macrocycle **1** in CBP (2.37 eV) is lower than that in Zeonex® (2.43 eV), and therefore the ΔE_{ST} of the material was reduced from 0.24 eV for Zeonex® to 0.18 eV for CBP, which indicates moderate exchange energy. The behavior of linear compound **2** was slightly different from that of **1**: the E_{T1} of **2** in Zeonex® (2.23 eV) is much higher than that in CBP host (2.11 eV) (Figure 6b and d). This would suggest that the triplet excited states of more structurally-flexible compound **2** is more influenced by the fluctuation of structural conformation than cyclic compound **1**. The polarity

of host matrix once again gave an impact on the ^{1}CT energy to decrease, thereby the ΔE_{ST} of **2** was narrowed from 0.25 eV in Zeonex® to 0.20 eV in CBP.

The intensity decay of the emission at different time delays were acquired for both compounds in Zeonex® and CBP hosts (Figure 7). In all cases, the PF and phosphorescence (PH) were observed at 80 K. Apparently, the decay curves of both compounds are typical for CT-based organic TADF emitters,[18a] and indeed, the DF process increased as the temperature elevated (Figure 7c and d, Figure S10e and f, and Figure S11e and f). However, with closer inspection, the temperature dependence of the decay profiles of **1** and **2** were different from each other: The DF process started at much lower temperature for macrocycle **1** (ca. 120 K) than for linear derivative **2** (ca. 200 K). This would indicate that higher activation energy is required for the rISC process in the case of **2**. Moreover, the rise of DF component in the case of **2** is much weaker than that of **1** (Figure 7b and d), indicating the less DF contribution to the PL of compound **2** in a host matrix. These results are also consistent with the results obtained with solutions (Figure 3c and d). Therefore, linear compound **2** exhibits lower device efficiency compared to macrocycle **1** (Figure 8, *vide infra*).

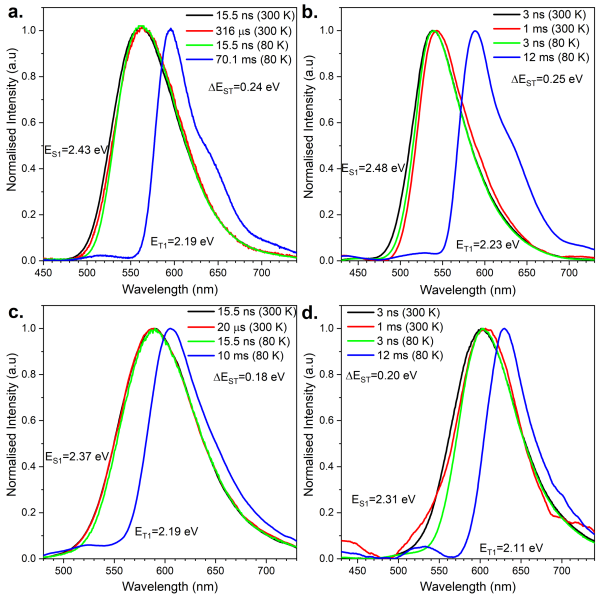

Figure 6. Normalized emission spectra of **1** and **2** in host matrices at varying delay times at 300 K and 80 K: (a) **1** and (b) **2** in Zeonex® (1 wt% in host matrix); (c) **1** and (d) **2** in CBP (10 wt% in host matrix).

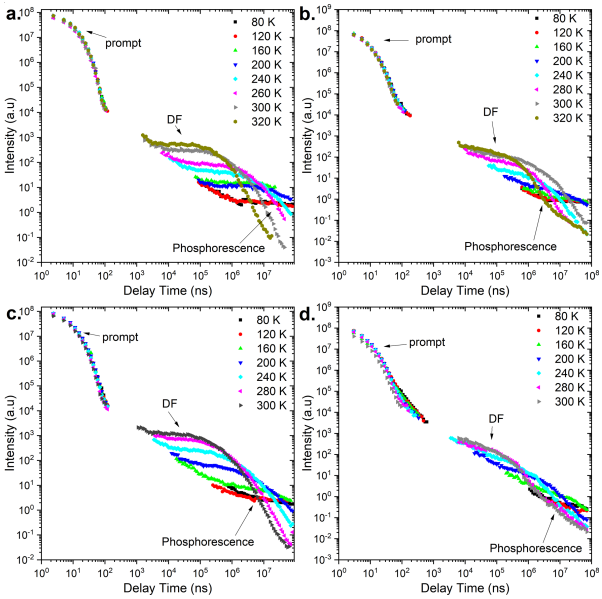

Figure 7. Emission intensities of **1** and **2** in host matrices against delay time measured at different temperature: (a) **1** and (b) **2** in Zeonex® (1 wt% in host matrix); (c) **1** and (d) **2** in CBP (10 wt% in host matrix).

Fabrication and Characteristics of OLED Devices. To investigate the possibility of applying **1** and **2** as OLED emitters, thermogravimetric analysis (TGA) of **1** and **2** were performed under air and N_2 (Figure S5 and S6 in the SI). High thermal decomposition temperatures [T_d (5 wt% loss) 548–585 °C for **1** and 535–578 °C for **2**] indicated that these molecules would be applicable to vacuum thermal deposition for purification and fabrication of OLEDs. To evaluate the validity of the macrocycle **1** and linear analog **2** as the TADF emitters, OLED devices were fabricated with **1** (DEV_1) and **2** (DEV_2) using the co-evaporation technique. The device structure fabricated was as follows: ITO/NPB (40 nm)/10 wt% TADF emitter (**1** or **2**) in CBP (30 nm)/TPBi (50 nm)/LiF (1 nm)/Al (100 nm). Both OLEDs fabricated with **1** and **2** showed a low turn-on voltage at 2.0 V and 2.5 V, respectively (Figure 8a). Importantly, the device fabricated with macrocycle **1** as the emitter displayed a bright orange emission (λ_{max} 589 nm) and far exceeded the theoretical maximum EQE of that with conventional fluorescent materials (5%), up to 11.6% (Figure 8b), clearly presenting a proof-of-concept of twisted D–A–D–A π-conjugated macrocyclic TADF emitter for OLEDs for the first time. More importantly, the EQE of the OLEDs fabricated with **1** also surpassed the maximum value of OLEDs fabricated with **2** (up to 6.9%, Figure 8b). The luminance of device fabricated with **1** was quite higher (> 23,000 cd m^{-2}) than that of **2** (ca. 12,500 cd m^{-2}), which suggested better charge recombination in the device based on **1** (Figure 8c). Both devices showed low-to-moderate efficiency roll-off (the roll-off of current efficiencies at 1,000 cd m^{-2} were 3.98% for **1** and 16.04% for **2**) (Figure 8d).

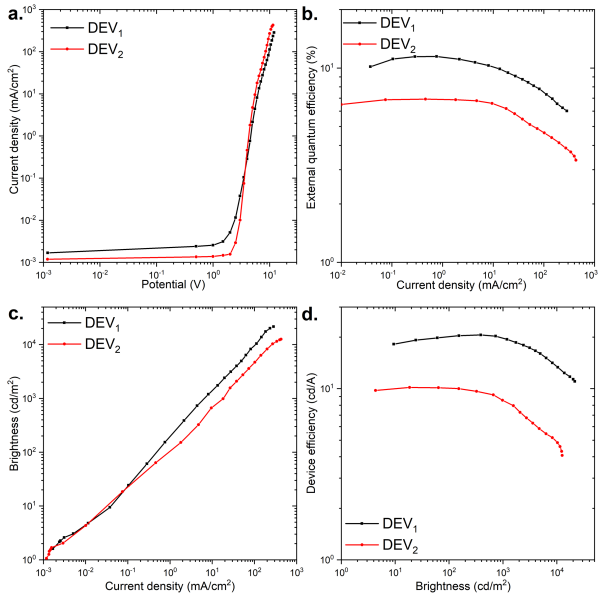

Figure 8. Device characteristics.

COCLUSION

We have succeeded in developing an efficient thermally activated delayed fluorescent D–A–D–A π-conjugated macrocycle based on rational molecular design, satisfying both of synthetic and functional requirements. The developed macrocycle forms two polymorphs with different color and emission color, depending on crystallization conditions. The X-ray crystallographic analyses and DFT calculations revealed the importance of molecular conformations and packing structures in different colors. It is noted that porous column structures assembled through intermolecular D•••A interactions in red crystal would be a peculiar feature of the D–A π-conjugated macrocycle. Comparative investigation of the physicochemical properties of the macrocycle with its linear analog has clearly demonstrated that the macrocyclization can be an effective strategy for increasing TADF contribution through the suppression of non-irradiative pathways. Most importantly, the first OLED device fabricated with a purely organic macrocyclic TADF emitter was realized, showing as high EQE as 11.6%. This exceeds the theoretical maximum of those fabricated with conventional fluorescent emitters (5%) and that with the linear analog (6.9%). We believe that this research opens up an avenue for designing new macrocyclic TADF materials. As a perspective, macrocyclic TADF emitters can provide great opportunities for tuning their photo- and redox properties through host-guest interactions.

ASSOCIATED CONTENT

Supporting Information. Supporting Information is available free of charge via the Internet at http://pubs.acs.org.
Experimental procedures for the syntheses of materials, spectroscopic data of new compounds, theoretical details including xyz files for coordinates, UV-Vis absorption and photoluminescence spectra, thermogravimetric analysis (TGA) profiles, and the copies of ^{1}H and ^{13}C NMR spectra of new compounds.

AUTHOR INFORMATION

Corresponding Authors

*przemyslaw.data@polsl.pl
*takeda@chem.eng.osaka-u.ac.jp
*minakata@chem.eng.osaka-u.ac.jp

Notes

The authors declare no competing financial interest.

ACKNOWLEDGMENT

This research was supported by the Grant-in-Aid for Scientific Research on Innovative Areas "π-System Figuration: Control of Electron and Structural Dynamism for Innovative Functions" (JSPS KAKENHI Grant No. JP17H05155 to Y.T.), "Aquatic Functional Materials: Creation of New Materials Science for Environment-Friendly and Active Functions" (JSPS KAKENHI Grant No. JP19H05716 to Y.T.), and the Continuation Grants for Young Researchers from the Asahi Glass Foundation (to Y.T.). P.D. acknowledges the kind support received from the First Team program of the Foundation for Polish Science co-financed by the European Union under the European Regional Development Fund (project number: First TEAM 2017-4/32 POIR.04.04.00-00-4668/17-00). Y.T. and P.D. acknowledge the EU's Horizon 2020 for funding the OCTA project under grant agreement No. 778158. We acknowledge the experimental supports of Professors Kei Tsujimoto (Osaka University) and Hiroshi Uyama (Osaka University) for the DSC measurement.

REFERENCES

(1) For selected reviews on π-conjugated linear oligomers and polymers in chemical sensors, see: (a) Rochat, S.; Swager, T. M. Conjugated Amplifying Polymers for Optical Sensing Applications. *ACS Appl. Mater. Interfaces* **2013**, *5*, 4488–4502. (b) Baek, P. Voorhaar, L.; Barker, D.; Travas-Sejdic, J. Molecular Approach to Conjugated Polymers with Biomimetic Properties. *Acc. Chem. Res.* **2018**, *51*, 1581–1589.

(2) For a review on π-conjugated linear oligomers and polymers in imaging, see: Wu, W.; Bazan, G. C.; Liu, B. Conjugated-Polymer-Amplified Sensing, Imaging, and Therapy. *Chem* **2017**, *2*, 760–790.

(3) For selected reviews on π-conjugated linear oligomers and polymers in OFETs, see: (a) Horowitz, G. Organic Field-Effect Transistors. *Adv. Mater.* **1998**, *10*, 365–377. (b) Wang, C.; Dong, H.; Hu, W.; Liu, Y.; Zhu, D. Semiconducting π-Conjugated Systems in Field-Effect Transistors: A Material Odyssey of Organic Electronics. *Chem. Rev.* **2012**, *112*, 2208–2267. (c) Mei, J.; Diao, Y.; Appleton, A. L.; Fang, L.; Bao, Z. Integrated Materials Design of Organic Semiconductors for Field- Effect Transistors. *J. Am. Chem. Soc.* **2013**, *135*, 6724–6746. (d) Osaka, I.; Takimiya, K. Naphthobischalcogenadiazole Conjugated Polymers: Emerging Materials for Organic Electronics. *Adv. Mater.* **2017**, *29*, 1605218.

(4) For selected reviews on π-conjugated linear oligomers and polymers in OPVs, see: (a) Günes, S.; Neugebauer, H.; Sariciftci N. S. Conjugated Polymer-Based Organic Solar Cells. *Chem. Rev.* **2007**, *107*, 1324–1338. (b) Cheng, Y.-J.; Yang, S.-H.; Hsu, C.-S. Synthesis of Conjugated Polymers for Organic Solar Cell Applications. *Chem. Rev.* **2009**, *109*, 5868–5923. (c) Lin, Y.; Li, Y.; Zhan, X. Small Molecule Semiconductors for High-Efficiency Organic Photovoltaics. *Chem. Soc. Rev.* **2012**, *41*, 4245–4272. (d) Dou, L.; You, J.; Hong, Z.; Xu, Z.; Li, G.; Street, R. A.; Yang, Y. 25th Anniversary Article: A Decade of Organic/Polymeric Photovoltaic Research. *Adv. Mater.* **2013**, *25*, 6642–6671. (e) Fu, H.; Wang, Z.; Sun, Y. Polymer Donors for High-Performance Non-Fullerene Organic Solar Cells. *Angew. Chem., Int. Ed.* **2019**, *58*, 4442–4453.

(5) For selected reviews on π-conjugated linear oligomers and polymers in OLEDs, see: (a) Kraft, A.; Grimsdale, A. C.; Holmes, A. B. Electroluminescent Conjugated Polymers—Seeing Polymers in a New Light. *Angew. Chem., Int. Ed.* **1998**, *37*, 402–428. (b) Mitschkea, U.; Bäuerle, P. The Electrolumi-

nescence of Organic Materials. *J. Mater. Chem.* **2000**, *10*, 1471–1507. (c) *Organic Light Emitting Devices: Synthesis, Properties and Applications*; Müllen, K., Scherf, U. Eds.; Wiley-VCH: Weinheim, 2006.

(6) (a) Kawase, T.; Kurata, H. Ball-, Bowl-, and Belt-Shaped Conjugated Systems and Their Complexing Abilities: Exploration of the Concave−Convex π-π Interaction. *Chem. Rev.* **2006**, *106*, 5250−5273. (b) Tahara, K.; Tobe, Y. Molecular Loops and Belts. *Chem. Rev.* **2006**, *106*, 5274−5290.

(7) (a) Höger, S. J. Highly Efficient Methods for the Preparation of Shape-Persistent Macrocyclics. *J. Polym. Sci., Part A: Polym. Chem.* **1999**, *37*, 2685−2698. (b) Zhang, W.; Moore J. S. Shape-Persistent Macrocycles: Structures and Synthetic Approaches from Arylene and Ethynylene Building Blocks. *Angew. Chem., Int. Ed.* **2006**, *45*, 4416–4439. (c) Diederich, F.; Kivala, M. All-Carbon Scaffolds by Rational Design. *Adv. Mater.* **2010**, *22*, 803–812. (d) Iyoda, M.; Yamalawa, J.; Rahman, M. J. Conjugated Macrocycles: Concepts and Applications. *Angew. Chem., Int. Ed.* **2011**, *50*, 10522–10533. (e) Iyoda, M.; Shimizu, H. Multifunctional π-Expanded Oligothiophene Macrocycles. *Chem. Soc. Rev.* **2015**, *44*, 6411–6424. (f) Smith, M. K.; Miljanić O. Š. Arylene Ethynylene Macrocycles: From Molecular Hosts to Components of High-Performance Supramolecular Architectures. *Org. Biomol. Chem.* **2015**, *13*, 7841–7845. (g) Lewis, S. E. Cycloparaphenylenes and Related Nanohoops. *Chem. Soc. Rev.* **2015**, *44*, 2221–2304.

(8) (a) Ball, M.; Nuckolls, C. Stepping into the Light: Conjugated Macrocycles with Donor–Acceptor Motifs. *ACS Cent. Sci.* **2015**, *1*, 416–417. (b) Ball, M.; Zhang, B.; Zhong, Y.; Fowler, B.; Xiao, S.; Ng, F.; Steigerwald, M.; Nuckolls, C. Conjugated Macrocycles in Organic Electronics. *Acc. Chem. Res.* **2019**, *52*, 1068–1078.

(9) (a) Chen, P.; Lalancette, R. A.; Jäkle, F. π-Expanded Borazine: An Ambipolar Conjugated B–π–N Macrocycle. *Angew. Chem., Int. Ed.* **2012**, *51*, 7994–7998. (b) Chen, P.; Yin, X.; Baser-Kirazli, N.; Jäkle, F. Versatile Design Principles for Facile Access to Unstrained Conjugated Organoborane Macrocycles. *Angew. Chem., Int. Ed.* **2015**, *54*, 10768–10772.

(10) (a) Darzi, E. R.; Hirst, E. S.; Weber, C. D.; Zakharov, L. N.; Lonergan, M. C.; Jasti, R. Synthesis, Properties, and Design Principles of Donor-Acceptor Nanohoops. *ACS Cent. Sci.* **2015**, *1*, 335–342. (b) Kuwabara, T.; Orii, J.; Segawa, Y.; Itami, K. Curved Oligophenylenes as Donors in Shape-Persistent Donor-Acceptor Macrocycles with Solvatofluorochromic Properties. *Angew. Chem., Int. Ed.* **2015**, *54*, 9646–9649.

(11) (a) Ball, M.; Fowler, B.; Li, P.; Joyce, L. A.; Li, F.; Liu, T.; Paley, D.; Zhong, Y.; Li, H.; Xiao, S.; Ng, F.; Steigerwald, M. L.; Nuckolls, C. Chiral Conjugated Corrals. *J. Am. Chem. Soc.* **2015**, *35*, 9982–9987. (b) Ball, M.; Zhong, Y.; Fowler, B.; Zhang, B.; Li, P.; Etkin, G.; Paley, D. W.; Decatur, J.; Dalsania, A. K.; Li, H.; Xiao, S; Ng, F.; Steigerwald, M. L.; Nuckolls, C. Macrocyclization in the Design of Organic n-Type Electronic Materials. *J. Am. Chem. Soc.* **2016**, *138*, 12861–12867. (c) Zhang, B.; Trinh, M. T.; Fowler, B.; Ball, M.; Xu, Q.; Ng, F.; Steigerwald, M. L.; Zhu, X.-Y.; Nuckolls, C.; Zhong, Y. Rigid, Conjugated Macrocycles for High Performance Organic Photodetectors. *J. Am. Chem. Soc.* **2016**, *138*, 16426−16431. (d) Zhang, B.; Hernández Sánchez, R.; Zhong, Y.; Ball, M.; Terban, M. W.; Paley, D.; Billinge, S. J. L.; Ng, F.; Steigerwald, M. L.; Nuckolls, C. Hollow Organic Capsules Assemble into Cellular Semiconductors. *Nat. Commun.* **2018**, *9*, 1957. (e) Ball, M. L.; Zhang, B.; Xu, Q.; Paley, D. W.; Ritter, V. C.; Ng, F.; Steigerwald, M. L.; Nuckolls, C. Influence of Molecular Conformation on Electron Transport in Giant, Conjugated Macrocycles. *J. Am. Chem. Soc.* **2018**, *140*, 10135−10139.

(12) For selected reviews on TADF, see (a) Tao, Y.; Yuan, K.; Chen, T.; Xu, P.; Li, H.; Chen, R.; Zheng, C.; Zhang, L.; Huang, W. Thermally Activated Delayed Fluorescence Materials Towards the Breakthrough of Organoelectronics. *Adv. Mater.* **2014**, *26*, 7931–7958. (b) Czerwieniec, R.; Leitl, M. J.; Homeier, H. H. H.; Yersin, H. Cu(I) Complexes – Thermally Activated Delayed Fluorescence. Photophysical Approach and Material Design. *Coord. Chem. Rev.* **2016**, *325*, 2–28. (c) Dias, F. B.; Penfold, T. J.; Monkman, A. P. Photophysics of Thermally Activated Delayed Fluorescence Molecule. *Methods Appl. Fluoresc.* **2017**, *5*, 012001. (d) Yang, Z.; Mao, Z.; Xie, Z.; Zhang, Y.; Liu, S.; Zhao, J.; Xu, J.; Chi, Z.; Aldred, M. P. Recent Advances in Organic Thermally Activated Delayed Fluorescence Materials. *Chem. Soc. Rev.* **2017**, *46*, 915–1016. (e) Wong, M. Y.; Zysman-Colman, E. Purely Organic Thermally Activated Delayed Fluorescence Materials for Organic Light-Emitting Diodes *Adv. Mater.* **2017**, *29*, 1605444. (f) Sarma, M.; Wong, K.-T. Exciplex: An Intermolecular Charge-Transfer Approach for TADF. *ACS Appl. Mater. Interfaces* **2018**, *10*, 19279–19304. (g) Chen, X.-K.; Kim, D.; Brédas, J.-L. Thermally Activated Delayed Fluorescence (TADF) Path toward Efficient Electroluminescence in Purely Organic Materials: Molecular Level Insight. *Acc. Chem. Res.* **2018**, *51*, 2215–2224. (h) Liu, Y.; Li, C.; Ren, Z.; Yan, S.; Bryce, M. R. All-Organic Thermally Activated Delayed Fluorescence Materials for Organic Light-Emitting Diodes. *Nat. Rev. Mater.* **2018**, *3*, 18020. (i) Data, P.; Takeda, Y. Recent Advancements in and the Future of Organic Emitters: TADF- and RTP-Active Multifunctional Organic Materials. *Chem. Asian J.* **2019**, *14*, 1613–1636.

(13) Endo, A.; Ogasawara, M.; Takahashi, A.; Yokoyama, D.; Kato, Y.; Adachi, C. Thermally Activated Delayed Fluorescence from Sn^{4+}-Porphyrin Complexes and Their Application to Organic Light-Emitting Diodes — A Novel Mechanism for Electroluminescence. *Adv. Mater.* **2009**, *21*, 4802–4806.

(14) Uchida, N.; Sato, T.; Kuwabara, J.; Nishimura, Y.; Kanbara, T. Delayed Fluorescence Behaviors of Aminopyridine Oligomers: Azacalix[*n*](2,6)pyridines (*n* = 3 and 4) and Their Linear Analog. *Chem. Lett.* **2014**, *43*, 459–461.

(15) Hu, Y.; Wang, Z.; Jiang, X.; Cai, X.; Su, S. J.; Huang, F.; Cao, Y. One-Step Synthesis of Cyclic Compounds towards Easy Room-Temperature Phosphorescence and Deep Blue Thermally Activated Delayed Fluorescence. *Chem. Commun.* **2018**, *54*, 7850–7853.

(16) Adachi, C.; Baldo, M. A.; Thompson, M. E.; Forrest, S. R. Nearly 100% Internal Phosphorescence Efficiency in an Organic Light Emitting Device. *J. Appl. Phys.* **2001**, *90*, 5048–5051.

(17) Takeda, Y.; Okazaki, M.; Minakata, S. Oxidative Skeletal Rearrangement of 1,1'-Binaphthalene-2,2'-diamines (BINAMs) via C‑C Bond Cleavage and Nitrogen Migration: a Versatile Synthesis of U-Shaped Azaacenes. *Chem. Commun.* **2014**, *50*, 10291–10294.

(18) (a) Data, P.; Pander, P.; Okazaki, M.; Takeda, Y.; Minakata, S.; Monkman, A. P. Dibenzo[*a*,*j*]phenazine-Cored Donor-Acceptor-Donor Compounds as Green-to-Red/NIR Thermally Activated Delayed Fluorescence Organic Light Emitters. *Angew. Chem., Int. Ed.* **2016**, *55*, 5739–5744. (b) Okazaki, M.; Takeda, Y.; Data, P.; Pander, P.; Higginbotham, H.; Monkman, A. P.; Minakata, S. Thermally Activated Delayed Fluorescent Phenothiazine-Dibenzo[*a*,*j*]phenazine-Phenothiazine Triads Exhibiting Tricolor-Changing Mechanochromic Luminescence. *Chem. Sci.* **2017**, *8*, 2677–2686. (c) Data, P.; Okazaki, M.; Minakata, S.; Takeda, Y. Thermally Activated Delayed Fluorescence *vs.* Room Temperature Phosphorescence by Conformation Control of Organic Single Molecules. *J. Mater. Chem. C* **2019**, *7*, 6616–6621. (d) Takeda, Y; Kaihara, T.; Okazaki, M.; Higginbotham, H.; Data, Przemyslaw; Tohnai, N.; Minakata, S. Conformationally-Flexible and Moderately Electron-Donating Units-Installed Donor-Acceptor-Donor Triad Enabling Multicolor-Changing Mechanochromic Luminescence, Thermally Activated Delayed Fluorescence, and

Room-Temperature Phosphorescence. *Chem. Commun*. **2018**, *54*, 6847–6850.

(19) Martí-Centelles, V.; Pandey, M. D.; Burguete, M. I.; Luis, S. V. Macrocyclization Reactions: The Importance of Conformational, Configurational, and Template-Induced Preorganization. *Chem. Rev.* **2015**, *115*, 8736–8834.

(20) Sobolev, A. N.; Belsky, V. K.; Romm, I. P.; Chernikova, N. Y.; Guryanova, E. N. Structural Investigation of the Triaryl Derivatives of the Group V Elements. IX. Structure of Triphenylamine, $C_{18}H_{15}N$. *Acta Crystallogr., Sect. C: Cryst. Struct. Commun.* **1985**, *41*, 967−971.

(21) (a) Chen, R.; Benicewicz, B. C. Preparation and Properties of Poly(methacrylamide)s Containing Oligoaniline Side Chains. *Macromolecules* **2003**, *36*, 6333–6339. (b) Eelkema, R.; Anderson, L. Synthesis of End-Functionalized Polyanilines. *Macromolecules* **2008**, *41*, 9930–9933.

(22) Kataoka, N.; Shelby, Q.; Stambuli, J. P.; Hartwig, J. F. Air Stable, Sterically Hindered Ferrocenyl Dialkylphosphines for Palladium-Catalyzed C−C, C−N, and C−O Bond-Forming Cross-Couplings. *J. Org. Chem.* **2002**, *67*, 5553–5566.

(23) Wang, C.; Li, Z. Molecular Conformation and Packing: Their Critical Roles in the Emission Performance of Mechanochromic Fluorescence Materials. *Mater. Chem. Front.* **2017**, *1*, 2174–2194.

(24) Yang, T.-F.; Chiu, K. Y.; Cheng, H. C.; Lee, Y. W.; Kuo, M. Y.; Su, Y. O. Studies on the Structure of *N*-Phenyl-Substituted Hexaaza[1_6]paracyclophane: Synthesis, Electrochemical Properties, And Theoretical Calculation. *J. Org. Chem.* **2012**, *77*, 8627−8633.

(25) Kuang, Z.; He, G.; Song, H.; Wang, X.; Hu, Z.; Sun, H.; Wan, Y.; Guo, Q.; Xia, A. Conformational Relaxation and Thermally Activated Delayed Fluorescence in Anthraquinone-Based Intramolecular Charge-Transfer Compound. *J. Phys. Chem. C* **2018**, *122*, 3727−3737.

(26) Wu, C.; Djurovich, P. I.; Thompson, M. E. Study of Energy Transfer and Triplet Exciton Diffusion in Hole-Transporting Host Materials. *Adv. Funct. Mater.* **2009**, *19*, 3157–3164.

(27) Yeh, S. J.; Tsai, C. Y.; Huang, C.-Y.; Liou, G.-S.; Cheng, S.-H. Electrochemical Characterization of Small Organic Hole-Transport molecules Based on the Triphenylamine Unit. *Electrochem. Commun*. **2003**, *5*, 373.

(28) de Silva, P.; Kim, C. A.; Zhu, T.; Voorhis, T. V. Extracting Design Principles for Efficient Thermally Activated Delayed Fluorescence (TADF) from a Simple Four-State Model. *Chem. Mater.* **2019**, *31*, 6995–7006.

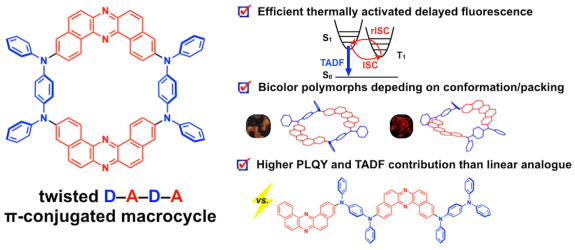
twisted D–A–D–A
π-conjugated macrocycle
Efficient thermally activated delayed fluorescence
S1
rISC
TADF
ISC
T1
S0
Bicolor polymorphs depeding on conformation/packing
Higher PLQY and TADF contribution than linear analogue
vs.